SUPPLEMENTARY INFORMATION

High entropy spinel oxide nanoparticles for visible light-assisted photocatalytic degradation of binary mixture of antibiotics in different water matrixes

Shubhasikha Das[a], Sudhir Kumar[b], Suman Sarkar[c], Debabrata Pradhan[b], Chandra Sekhar Tiwary[d]*, Shamik Chowdhury[a]*,

[a]School of Environmental Science and Engineering,
Indian Institute of Technology Kharagpur, West Bengal 721302, India

[b]Materials Science Centre,
Indian Institute of Technology Kharagpur, West Bengal 721302, India

[c]Department of Materials Engineering,
Indian Institute of Technology Jammu, Jammu 181221, India

[d]Department of Metallurgical and Materials Engineering,
Indian Institute of Technology Kharagpur, West Bengal 721302, India

* Corresponding author.

E-mail address: chandra.tiwary@metal.iitkgp.ac.in (C. S. Tiwary)
shamikc@iitkgp.ac.in (S. Chowdhury)

Table S1 Basic characteristics of the various real water matrixes.

Parameters	Unit	DI	TW	GW	SW	MWW	HWW	PWW	T-MWW	Methodology
pH	–	6.5	7.7	7.1	6.9	6.7	7.2	4.17	6.11	IS 3025 (Part 11), 1983 APHA (*23rd edition*), 4500 H^+ B
Turbidity	NTU	–	1.4	2.2	7.2	72.8	23.5	3.4	1.9	IS 3025 (Part 10), 1984 APHA (*23rd edition*), 2130 B
Total dissolved solid (TDS)	mg L^{-1}	–	155	–	146	395	255	9129	320	IS 3025 (Part 16), 1984 APHA (*23rd edition*), 2540C
Total suspended solid (TSS)	mg L^{-1}	–	2.2	56	51	88	46	22	7.3	IS 3025 (Part 17), 1984 APHA (*23rd edition*), 2540 D
Biological oxygen demand (BOD)	mg L^{-1}	–	3.5	6	8	206	124	15	15	IS 3025 (Part 44), 1993
Chemical oxygen demand (COD)	mg L^{-1}	–	5.3	81	34	172	61	532	76	APHA (*23rd edition*), 5220 B
Chloride (Cl^-)	mg L^{-1}	–	32	5	41	56	81	58	65	IS:3025 (Part 32), 1988 APHA (*23rd edition*), 4500 Cl^- B
Nitrate (NO_3^-)	mg L^{-1}	–	8	7.8	12	42	52	21	14	APHA (*23rd edition*), 3500 NO_3^-
Bicarbonate (HCO_3^-) as	mg L^{-1}	–	57	26	64	218	276	–	13	APHA (*23rd edition*), 2320 B

$CaCO_3$										
Sulpahte (SO_4^{2-})	mg L^{-1}	–	17	5.2	21	44	31	28	23	IS:3025(Part 24), 1986 APHA (*23^rd^ edition*), 4500 SO_4^{2-} E
Phosphate (PO_4^{3-}) as P	mg L^{-1}	–	0.6	–	51	49	57	382	2	APHA (*23^rd^ edition*), 4500 PO_4^{3-} D

Table S2 Specific surface area of FeCoNiCuZn and $(FeCoNiCuZn)_aO_b$ NPs, as determined by the multipoint Brunauer–Emmett–Teller method.

Sample	**SSA (m^2 g^{-1})**
FeCoNiCuZn	19
$(FeCoNiCuZn)_aO_b$_250	23
$(FeCoNiCuZn)_aO_b$_350	40
$(FeCoNiCuZn)_aO_b$_450	54
$(FeCoNiCuZn)_aO_b$_550	67

Table S3 Elemental composition (at.%) of $(FeCoNiCuZn)_aO_b$ NPs based on EDS analysis.

Sample	**Fe**	**Co**	**Ni**	**Cu**	**Zn**	**O**
$(FeCoNiCuZn)_aO_b$_250	12.55	11.33	11.26	14.23	10.40	40.23
$(FeCoNiCuZn)_aO_b$_350	11.90	11.03	10.55	13.95	9.14	43.43
$(FeCoNiCuZn)_aO_b$_450	11.23	10.65	10.28	12.19	8.97	46.68
$(FeCoNiCuZn)_aO_b$_550	10.44	9.99	9.61	11.10	8.31	50.55

Table S4 Comparison of the photocatalytic performance of $(FeCoNiCuZn)_aO_b$_550 NPs for degradation of SMX and OFX with contemporary semiconductor-based photocatalysts.

Photocatalyst	C_0 (mg L^{-1})	Time (min)	Dose (g L^{-1})	Irradiance type	Degradation (%)	k ($\times 10^{-3}$ min^{-1})	Reference
Sulfamethoxazole							
ZnO	10	90	0.3	Visible light	20	10.2	1
Cu_2O	3	30	0.4	Visible light	48	–	2
Fe_2O_3	10	90	0.3	Visible light	52	–	1
$CuFeS_2$– dendritic mesoporous silica-titania/persulfate	10	140	1.2	Visible light	89	14.6	3
N–$SrTiO_3$/$NH_4V_4O_{11}$	50	120	2.0	Visible light	91	13.2	4
Co-CuS@TiO_2	5	120	0.25	Visible light	100	21.6	5
N–ZnO/C@ Bi_2MoO_6	5	120	1.0	Visible light	93	25.1	6
FeCoNiCuZn	5	120	0.5	Visible light	94	19.5	7
MnFeCoNiCu	5	120	0.5	Visible light	95	22	8
$(FeCoNiCuZn)_aO_b$_550	5	90	0.5	Visible light	97	31.9	This study

Ofloxacin							
WO_3	10	240	0.25	UV(c) light	50	2.2	9
α-Fe_2O_3	20	60	0.1	Visible light	56	14.0	10
ZnO	30	180	0.25	Visible light	57	8.2	11
Cu-doped TiO_2	10	180	0.45	Visible light	72	4.5	12
Bi/Ni co-doped TiO_2	25	360	1.5	Visible light	86	6.2	13
Bi_2MoO_6-rGO-TiO_2	4×10^{-5} M	120	0.4	Visible light	92	17.4	14
$BiFeO_3$/Bi-g-C_3N_4	10	90	0.25	Visible light	96	34.4	15
MnFeCoNiCu	5	120	0.5	Visible light	94	21	8
$(FeCoNiCuZn)_aO_b$_550	5	90	0.5	Visible light	95	26.7	This study

Table S5 Major intermediates formed during photocatalytic degradation of SMX over $(FeCoNiCuZn)_aO_b$_550 NPs, as detected through LCMS.

Intermediate	*m*/*z*	Molecular formula	Chemical structure	Chemical name
S1	276	$C_9H_{13}N_3O_5S$	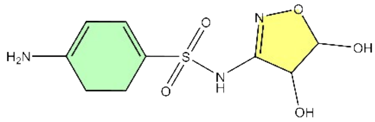	4-amino-*N*-(4,5-dihydroxy-4,5-dihydroisoxazol-3-yl)cyclohexa-1,3-diene-1-sulfonamide
S8	177	$C_4H_6N_2O_4S$	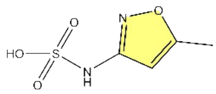	4-hydroxybenzene-1-sulfonamide
S3	171	$C_6H_8N_2O_2S$	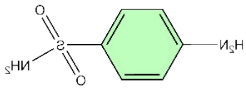	4-amino benzenesulfonamide
S4	118	$C_4H_6O_4$	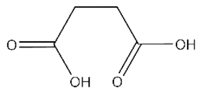	succinic acid
S5	156	$C_6H_7NO_2S$	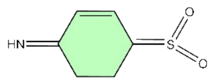	4-sulfonylcyclohex-2-en-1-imine
S6	99	$C_4H_6N_2O$	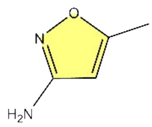	5-methylisoxazol-3-amine
S7	127	$C_4H_4N_2O_3$	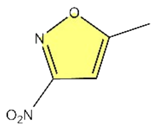	5-methyl-3-nitroisoxazole
S8	122	$C_4H_9NO_3$	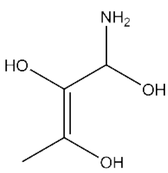	(E)-1-aminobut-2-ene-1,2,3-triol
S9	102	$C_4H_7NO_2$	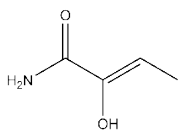	(Z)-2-hydroxybut-2-enamide

S10	94	C_6H_7N	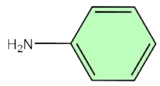	Aniline
S11	60	C_3H_6O	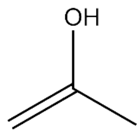	prop-1-en-2-ol

Table S6 Major intermediates formed during photocatalytic degradation of OFX over $(FeCoNiCuZn)_aO_b$_550 NPs, as detected through LCMS.

Intermediate	*m*/*z*	Molecular formula	Chemical structure	Chemical name
O1	349	$C_{17}H_{18}FN_3O_4$	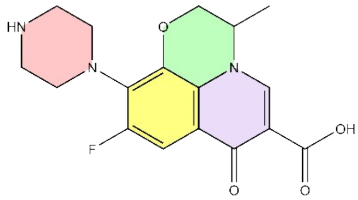	9-fluoro-3-methyl-7-oxo-10-(piperazin-1-yl)-3,7-dihydro-2*H*-[1,4]oxazino[2,3,4-*ij*]quinoline-6-carboxylic acid
O2	327	$C_{17}H_{17}N_3O_4$	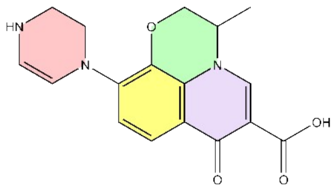	3-methyl-7-oxo-10-(piperazin-1-yl)-3,7-dihydro-2*H*-[1,4]oxazino[2,3,4-*ij*]quinoline-6-carboxylic acid
O3	290	$C_{15}H_{16}FN_3O_2$	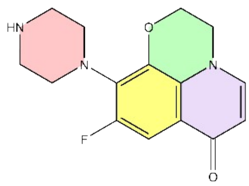	9-fluoro-10-(piperazin-1-yl)-2,3-dihydro-7*H*-[1,4]oxazino[2,3,4-*ij*]quinolin-7-one
O4	251	$C_{13}H_{15}FN_2O_2$	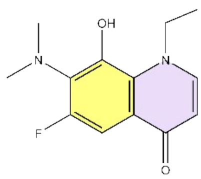	7-(dimethylamino)-1-ethyl-6-fluoro-8-hydroxyquinolin-4(1*H*)-on
O5	235	$C_{13}H_{16}N_2O_2$	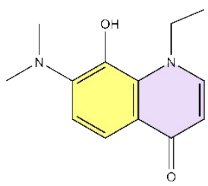	7-(dimethyl amino)-1-ethyl-8-hydroxyquinolin-4 (1*H*)-one
O6	177	$C_{10}H_{13}NO_2$	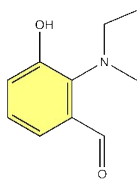	2-(ethy l(methyl)amino)-3-hydroxybenzaldehy de

O7	211	$C_{10}H_{11}FN_2O_2$	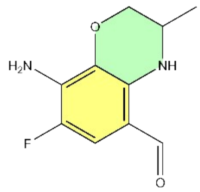	8-amino-7-fluoro-3-methyl-3,4-dihydro-2*H*-benzo[b][1,4] oxazine-5carbaldehyde
O8	148	$C_7H_{15}FN_2$	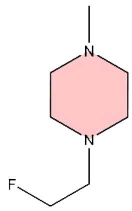	1-(2-fluoroethyl)-4-methylpiperazine
O9	101	$C_5H_{12}N_2$	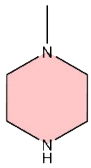	1-methylpiperazine
O10	127	$C_5H_8N_2O_2$	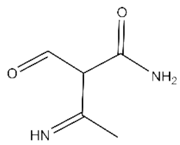	2-formyl-3-iminobutanamide
O11	117	$C_4H_4O_4$	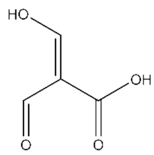	(E)-2-formyl-3-hydroxyacrylic acid
O12	87	$C_5H_{13}N$	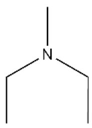	*N*-ethyl-*N*-methylethanamine
O13	73	$C_3H_4O_2$	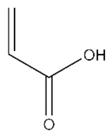	acrylic acid

Table S7 Leached metal ion concentration (in μg L^{-1}) after photocatalytic degradation of SMX and OFX over $(FeCoNiCuZn)_aO_b$_550 NPs under visible light irradiation.

	Fe^{2+}	Co^{2+}	Ni^{2+}	Cu^{2+}	Zn^{2+}
SMX	5	280	245	125	10
OFX	BDL*	220	289	245	85

*BDL: Below detection limit

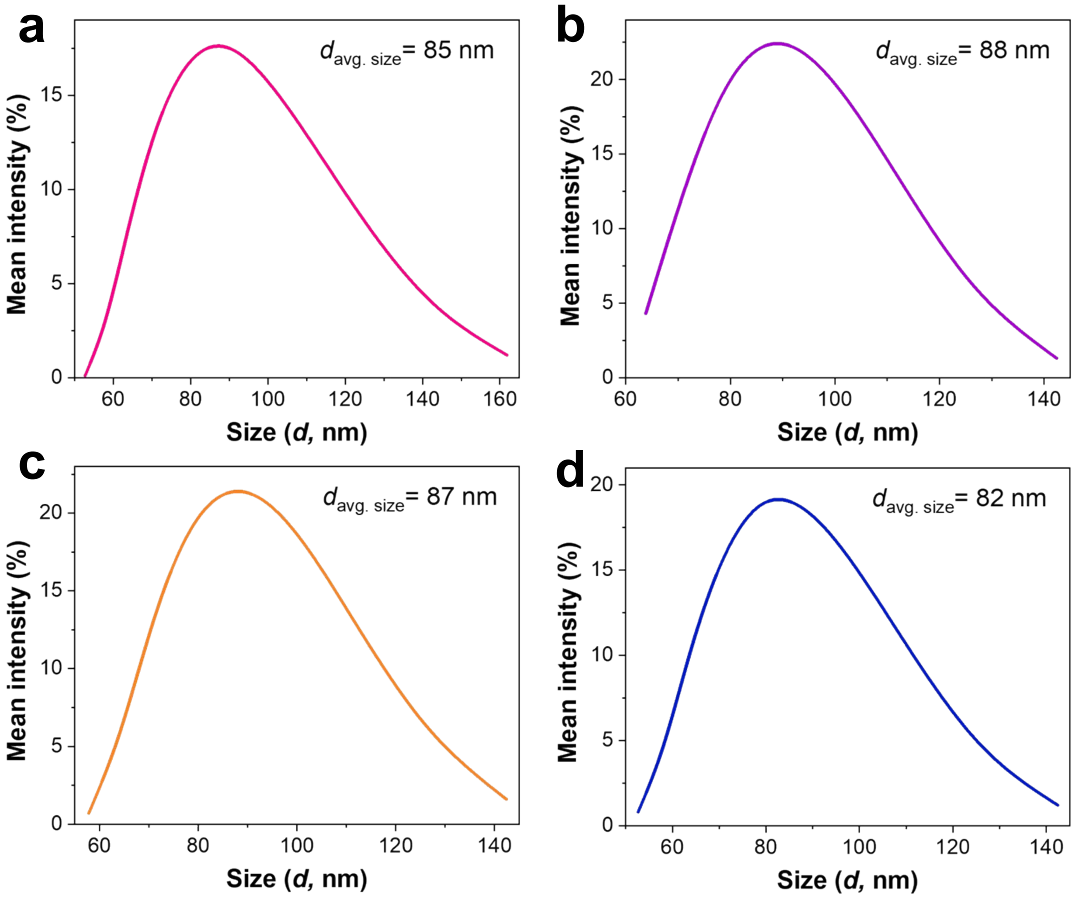

Figure S1 Particle size distributions of (a) $(FeCoNiCuZn)_aO_b$_250 NPs, (b) $(FeCoNiCuZn)_aO_b$_350 NPs, (c) $(FeCoNiCuZn)_aO_b$_450 NPs, and (d) $(FeCoNiCuZn)_aO_b$_550 NPs.

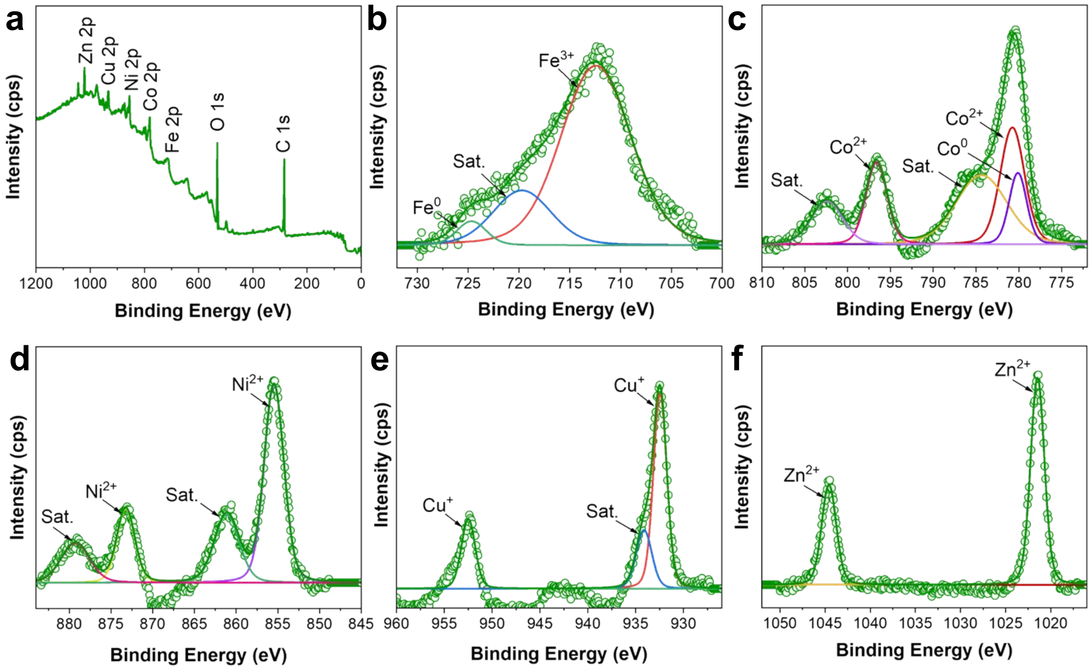

Figure S2 (a) XPS survey scan and the deconvoluted high-resolution (b) Fe 2p (c) Co 2p, (d) Ni 2p, (e) Cu 2p, and (g) Zn 2p spectra of pristine FeCoNiCuZn NPs.

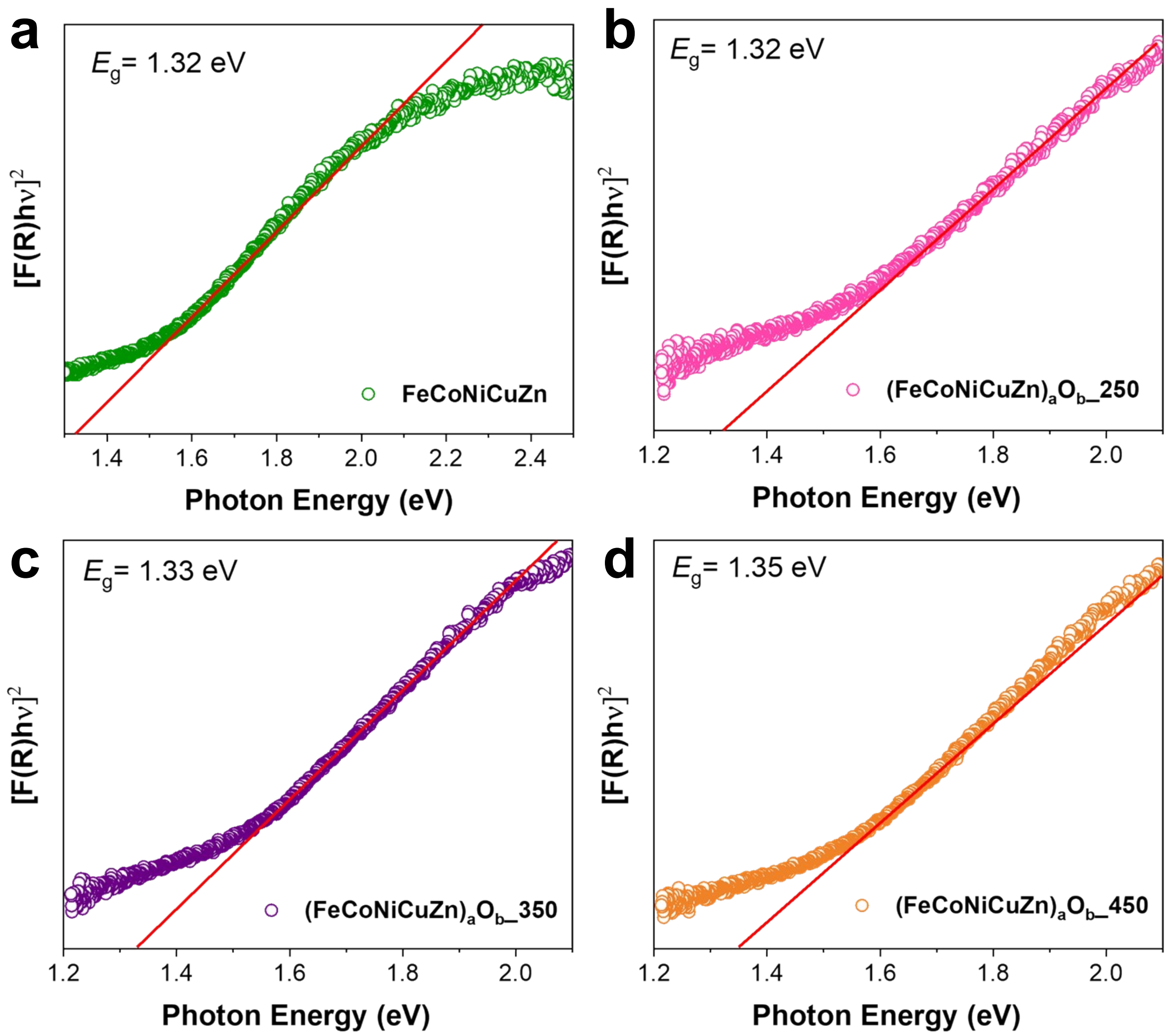

Figure S3 Kubelka–Munk plots of (a) FeCoNiCuZn NPs, (b) $(FeCoNiCuZn)_aO_b$_250 NPs, (c) $(FeCoNiCuZn)_aO_b$_350 NPs, and (d) $(FeCoNiCuZn)_aO_b$_450 NPs for estimating the bandgap energy.

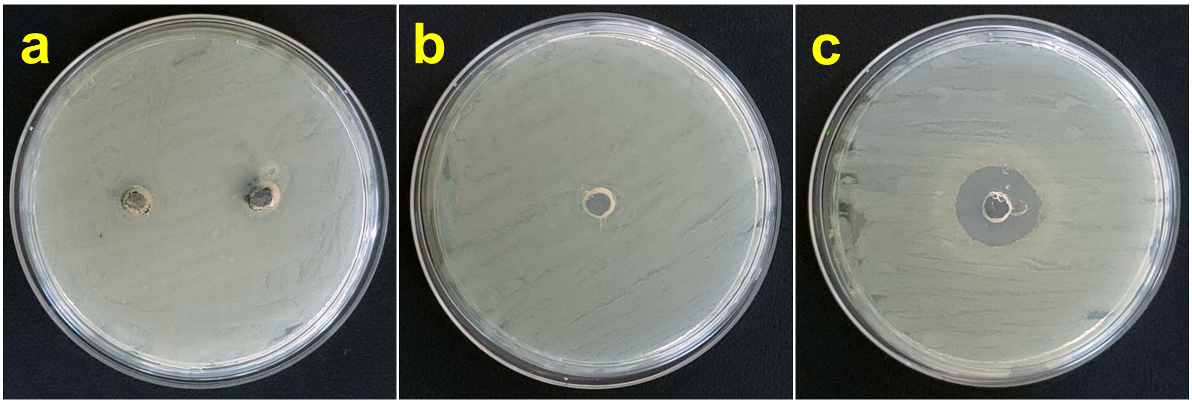

Figure S4 Digital images illustrating the results of agar-well diffusion assay for toxicity assessment of $(FeCoNiCuZn)_aO_b$_550 NPs (a), with PBS as negative control (b) and CFX as positive control (c).

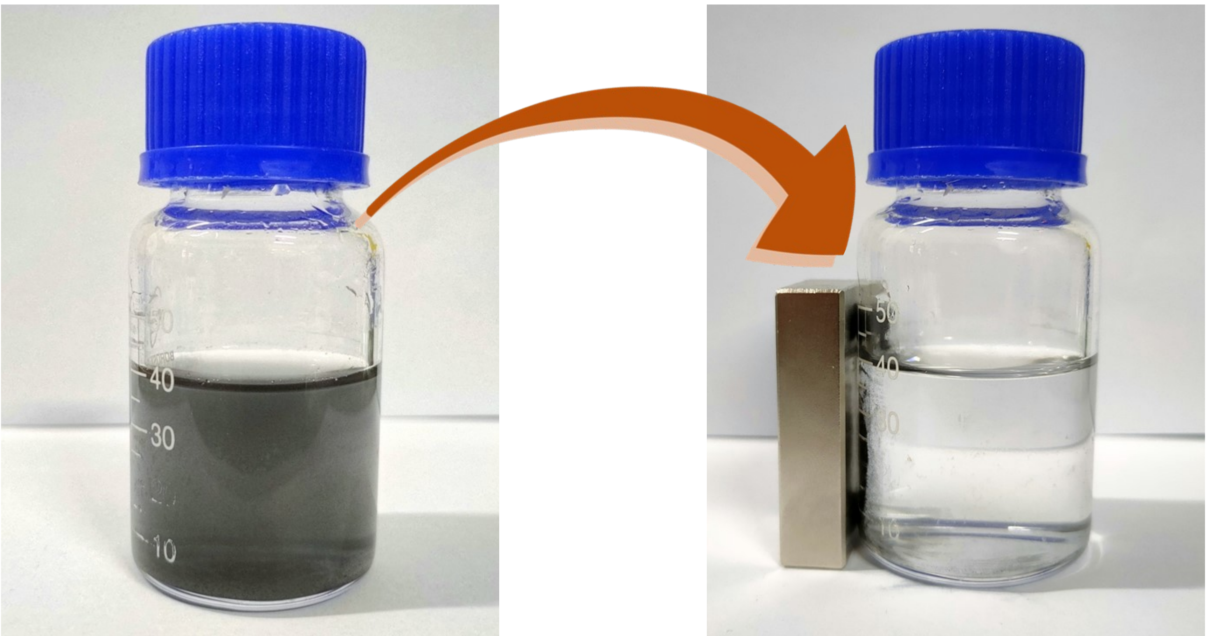

Figure S5 Digital images illustrating the magnetic separation of $(FeCoNiCuZn)_aO_b$_550 NPs from aqueous solution.

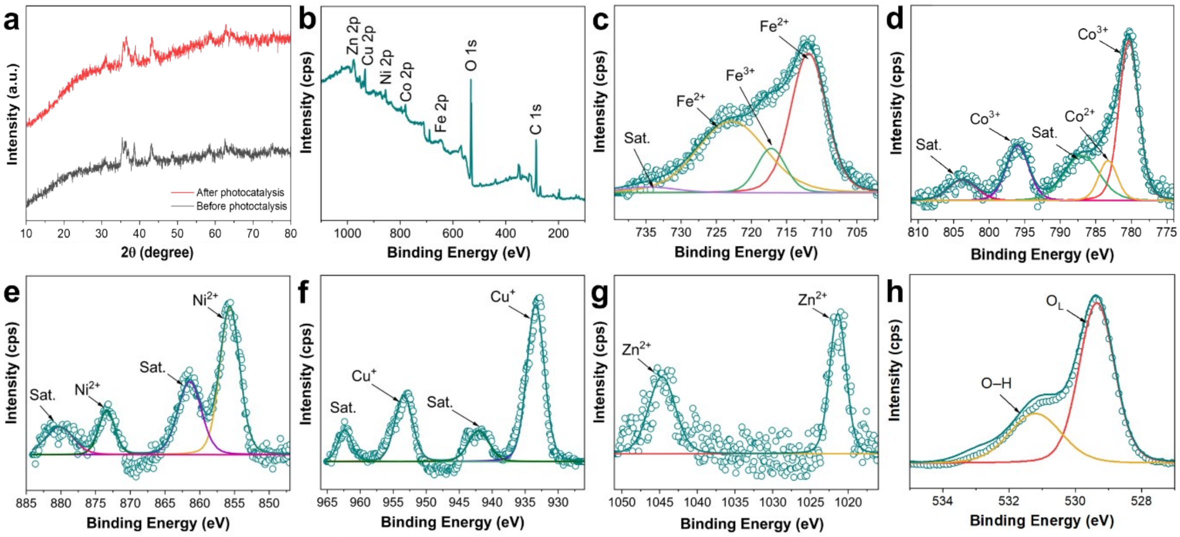

Figure S6 (a) Comparison of the XRD patterns of $(FeCoNiCuZn)_aO_b$_550 NPs before and after three consecutive photocatalytic runs. (b) XPS survey scan and the deconvoluted high-resolution (c) Fe 2p (d) Co 2p, (e) Ni 2p, (f) Cu 2p, (g) Zn 2p, and (h) O 1s spectra of $(FeCoNiCuZn)_aO_b$_550 NPs after three consecutive photocatalytic runs.

References

1 P. Dhiman, A. Kumar, M. Shekh, G. Sharma, G. Rana, D. V. N. Vo, N. AlMasoud, M. Naushad and Z. A. ALOthman, *Environ. Res.*, 2021, **197**, 111074.

2 K. Sekar, C. Chuaicham, B. Vellaichamy, W. Li, W. Zhuang, X. Lu, B. Ohtani and K. Sasaki, *Appl. Catal. B Environ.*, 2021, **294**, 120221.

3 T. S. Ntelane, U. Feleni, N. H. Mthombeni and A. T. Kuvarega, *J. Colloid Interface Sci.*, 2024, **654**, 660–676.

4 Y. Zhang, Y. Li and Y. Yuan, *J. Colloid Interface Sci.*, 2023, **645**, 860–869.

5 O. Mertah, A. Gómez-Avilés, A. Slassi, A. Kherbeche, C. Belver and J. Bedia, *Catal. Commun.*, 2023, **175**, 106611.

6 A. Wang, J. Ni, W. Wang, X. Wang, D. Liu and Q. Zhu, *J. Hazard. Mater.*, 2022, **426**, 128106.

7 S. Das, M. Sanjay, A. R. Singh Gautam, R. Behera, C. S. Tiwary and S. Chowdhury, *J. Environ. Manage.*, 2023, **342**, 118081.

8 S. Das, M. Sanjay, S. Kumar, S. Sarkar, C. S. Tiwary and S. Chowdhury, *Chem. Eng. J.*, 2023, **476**, 146719.

9 J. Piriyanon, P. Takhai, S. Patta, T. Chankhanittha, T. Senasu, S. Nijpanich, S. Juabrum, N. Chanlek and S. Nanan, *Opt. Mater.*, 2021, **121**, 111573.

10 H. Alamgholiloo, N. Noroozi Pesyan and A. Poursattar Marjani, *Sep. Purif. Technol.*, 2023, **305**, 122442.

11 H. Cai, J. Wang, Z. Du, Z. Zhao, Y. Gu, Z. Guo, Y. Huang, C. Tang, G. Chen and Y. Fang, *Colloids Surfaces A Physicochem. Eng. Asp.*, 2023, **663**, 131050.

12 R. Kaur, A. Kaur, R. Kaur, S. Singh, M. S. Bhatti, A. Umar, S. Baskoutas and S. K. Kansal, *Adv. Powder Technol.*, 2021, **32**, 1350–1361.

13 V. Bhatia, A. K. Ray and A. Dhir, *Sep. Purif. Technol.*, 2016, **161**, 1–7.

14 A. Raja, N. Son and M. Kang, *Environ. Res.*, 2021, **199**, 111261.

15 S. H. Ammar, F. D. Ali, H. J. Hadi and Z. H. Jabbar, *Mater. Sci. Semicond. Process.*, 2024, **171**, 108026.